CrossMark

Co-generation of electricity and chemicals from propane fuel in solid oxide fuel cells with anode containing nano-bimetallic catalyst

Lei Zhang [a], Chenghao Yang [a,b], Anatoly I. Frenkel [c], Siwei Wang [a], Guoliang Xiao [a], Kyle Brinkman [d], Fanglin Chen [a,*]

[a] Department of Mechanical Engineering, University of South Carolina, Columbia, SC 29208, USA
[b] Energy Research Institute, College of Environment and Energy, South China University of Technology, Guangzhou 510640, PR China
[c] Department of Physics, Yeshiva University, New York, NY 10016, USA
[d] Science and Technology Directorate, Savannah River National Laboratory, Aiken, SC 29808, USA

H I G H L I G H T S

- $Pr_{0.4}Sr_{0.6}Co_{0.2}Fe_{0.7}Nb_{0.1}O_{3-\delta}$ was used as an anode in direct propane fueled SOFCs.
- Co–Fe bimetallic phase was formed from $Pr_{0.4}Sr_{0.6}Co_{0.2}Fe_{0.7}Nb_{0.1}O_{3-\delta}$ SOFC anode.
- High cell performance was obtained for SOFCs with anode containing Co–Fe catalysts.
- Polycyclic aromatic hydrocarbons were produced from SOFCs using propane as fuel.

A R T I C L E I N F O

A B S T R A C T

The perovskite material $Pr_{0.4}Sr_{0.6}Co_{0.2}Fe_{0.7}Nb_{0.1}O_{3-\delta}$ was used as an anode in direct propane fueled solid oxide fuel cells (SOFCs). After exposure of the initial single phase $Pr_{0.4}Sr_{0.6}Co_{0.2}Fe_{0.7}Nb_{0.1}O_{3-\delta}$ to a reducing atmosphere at 900 °C, it transformed to a two-phase system with nano-particles of a Co–Fe bimetallic alloy uniformly distributed on a Ruddlesden–Popper ceramic phase. High cell power output and good stability were obtained using propane as the fuel and ambient air as the oxidant. Due to the catalytic effect of the Co–Fe bimetallic alloy in the SOFC operating conditions, macromolecular compounds of polycyclic aromatic hydrocarbons (PAHs) were generated as by-products in the exhaust stream of the anode. This novel anode system successfully demonstrated the co-generation of electricity and high value end use chemicals from direct hydrocarbon fueled SOFC systems.

© 2014 Elsevier B.V. All rights reserved.

1. Introduction

Solid oxide fuel cells (SOFCs) are solid state devices which can convert the chemical energy in a fuel directly into electricity [1,2]. It is attractive to carry out chemical synthesis in SOFCs to co-generate electricity from the excess free energy of the reaction [3,4]. The experimental evidence of the chemical co-generation in SOFCs was first demonstrated by Farr and Vayenas with the production of nitric oxide from oxidation of ammonia and recovering part of the emitted energy as electricity [5]. Co-generation processes to oxidation reaction of H_2S to SO_2 and partial oxidation of methanol

to formaldehyde on SOFCs have also been studied by the Vayenas group [6,7]. Generally, the co-generated chemical by-products are H_2, H_2O, CO, CO_2 and some small molecular hydrocarbons [8,9]. This kind of co-generation of synthesis gas (syngas) and electrical power is an efficient technology for energy conversion. However, the traditional co-generated chemical by-product syngas is in the gaseous state under ambient temperature and pressure which poses problems for capture, storage and transport. There has been no report on macromolecular compounds such as polycyclic aromatic hydrocarbons (PAHs) produced from hydrocarbon in SOFCs. PAHs containing a benzene ring usually occur in oil, coal, and tar deposits, and are produced as by-products of fuel burning (fossil fuel or biomass) [10,11]. Interestingly, PAHs are typically liquids at ambient temperature and pressure which make them convenient for capture, storage and transport. If PAHs could be synthesized via

electrochemical reactions in SOFCs, it would lead to a significant improvement in the co-generation processes and further our understanding of electrochemical phenomena that occur in high temperature fuel cell systems.

The electrochemical oxidation reaction of hydrocarbon species occurs on the anode side, which is one of the most important reactions in SOFCs [12]. For direct hydrocarbon fueled SOFCs, different anode materials have been reported [13]. Conventional Ni-based materials combined with doped ceria [14,15] or BaO [16], Cu-based material [17], noble metals [18] and various perovskites [19,20] or double perovskites [21] have been demonstrated as potential anode materials for hydrocarbon fueled SOFCs. Recently a redox-reversible anode material based on the perovskite $Pr_{0.4}Sr_{0.6}Co_{0.2}Fe_{0.7}Nb_{0.1}O_{3-\delta}$ (PSCFN) has been discovered by our group [22]. It was observed that a nanosized Co–Fe alloy (CFA) was formed in-situ after exposing PSCFN to reducing atmospheres at 900 °C. It has been demonstrated that this dual-phase anode material can directly oxidize hydrocarbons without suffering from coking and is tolerant to sulfur impurities in the fuel stream at relatively high concentrations. This study focused on the following two important aspects: i) the composition and structure of the CFA was further studied to help evaluate the performance of bimetallic catalysis and ii) the dual phase anode containing CFA was demonstrated as a unique anode material for the co-generation of high value end use chemicals from direct hydrocarbon fueled SOFC systems.

Cobalt and iron are common transition metals used as catalysts for the Fischer–Tropsch synthesis [23,24]. The Fischer–Tropsch synthesis is a collection of chemical reactions that convert a mixture of carbon monoxide and hydrogen into hydrocarbons [25]. Hydrocarbon products which are in liquid state at standard temperature and pressure are desired for the convenience of capture, storage and transport [26]. Generally, the Fischer–Tropsch synthesis is operated in the temperature range of 150–300 °C with alkanes, alcohols, and other oxygenated hydrocarbons as the common products [27]. In contrast, the SOFC systems in this study operate in the temperature range of 750–850 °C. The elevated temperatures coupled with the electrochemical nature of the reactions are expected to produce different hydrocarbon products than the low temperature conventional chemical synthesis processes. Due to highly active CFA nano-particles on the PSCFN, it is likely to co-synthesize other chemicals while operating SOFCs with this anode material in hydrocarbon fuels.

In this work, novel PSCFN was used as an anode for the direct use of propane (with 3 vol% H_2O) in SOFCs. High electrochemical performance was achieved with appreciable stability. High value end use chemicals such as PAHs were produced as products from the co-generation of electricity and chemicals, attributed to the Co–Fe bimetallic alloy catalytic activity and the electrochemical reactions occurring at elevated temperature in the SOFC systems.

2. Experimental

2.1. Material preparation and cell fabrication

$Pr_{0.4}Sr_{0.6}Co_{0.2}Fe_{0.7}Nb_{0.1}O_{3-\delta}$ (PSCFN) powders were synthesized by a citrate combustion method, using $Pr(NO_3)_3$, $Sr(NO_3)_2$, $Fe(NO_3)_3$, $Co(NO_3)_2$, and $C_4H_4NNbO_9$ solution as precursors. Citrate acid was added as a chelating agent and combustion enhancer. After heating the solution into a gel on a hotplate at 100 °C while stirring, a microwave oven was used for further heating until self-combustion occurred, yielding a homogeneous black powder. A calcination step was performed by firing the as-synthesized powders to 1000 °C for 2 h to remove the residual organic content and to result in the single crystalline perovskite phase.

$La_{0.8}Sr_{0.2}Ga_{0.83}Mg_{0.17}O_{3-\delta}$ (LSGM) [28] and $Ba_{0.9}Co_{0.7}Fe_{0.2}Nb_{0.1}O_{3-\delta}$ (BCFN) [29] powders used as the electrolyte and the cathode were synthesized using a solid state reaction method.

Single SOFC cells were fabricated with an electrolyte supported configuration with screen-printed electrodes. The electrolyte substrates were prepared by pressing the LSGM powders and subsequently sintering at 1400 °C for 5 h. The sintered LSGM substrates were about 10.5 mm in diameter and 0.3 mm thick. The electrode slurry of PSCFN and BCFN was prepared by mechanically mixing the electrode powders with a Heraeus binder V-006, respectively. The electrode slurry was screen-printed onto each side of the electrolyte substrate and fired at 1000 °C for 2 h to form porous electrodes. Au and Pt slurry was printed on the surface of the anode and cathode, respectively to serve as a current collector [22].

2.2. Characterization

The crystalline structure of the powder samples was identified by powder X-ray diffraction (XRD) with a Rigaku D/Max 2100 Powder X-ray Diffractometer. The microstructure of the powder samples was obtained by a scanning electron microscope (SEM) technique using a FEI Quanta 200 environmental scanning electron microscope and a high-resolution transmission electron microscopy (HRTEM, Fei Tecnai F30) with a point-to-point resolution of 0.21 nm operated at 300 kV and the elemental distributions of the samples were characterized under STEM mode by an energy dispersive spectroscopy (EDS) analyzer.

In order to detect the formation of the Co–Fe bimetallic alloy, X-ray absorption fine structure (XAFS) experiments were performed on the reduced PSCFN powders (reduced in H_2 at 900 °C for 5 h) using the X18B and X19A beamlines at the National Synchrotron Light Source (NSLS), Brookhaven National Laboratory. Specimens were prepared by brushing the powders on the adhesive tape and then folding several times to make a uniform sample for transmission XAFS experiment. XAFS data were collected at the Co K edge (7709 eV) and Fe K edge (7112 eV) using a transmission method in air at room temperature. For comparison, the XAFS data of standard Co (Co K edge 7709 eV) and Fe (Fe K edge 7112 eV) metal foils were also collected.

The chemicals collected in the anode exhaust stream of direct propane fueled SOFCs were analyzed by gas chromatography and mass spectrometry (GC–MS) and data was acquired on a VG70S
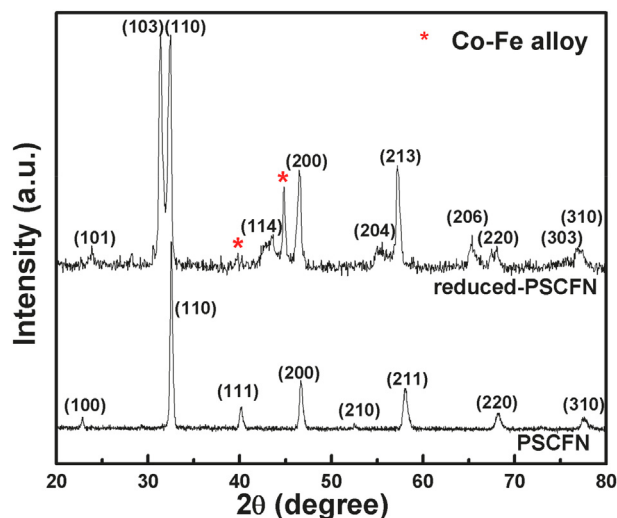

Fig. 1. XRD of PSCFN powders before and after exposure to reducing conditions (H_2 900 °C/5 h).

magnetic sector mass spectrometer by both direct probe introduction and by GC—MS. Electron impact ionization methods were used for detection in both methods. The GC column used a 30 m Rtx-5 and was programmed from 80 °C to 300 °C at 10 °C min^{-1}. The chemicals were also analyzed by nuclear magnetic resonance (NMR) using a Bruker AVANCE DRX 400 MHz NMR spectrometer. Fourier Transform Infrared Spectrometry (FTIR) spectra were recorded on a PerkinElmer spectrum 100 FTIR spectrometer.

2.3. Cell testing

Electrochemical measurements were conducted with a Versa STAT 3-400 electrochemical workstation (Princeton Applied Research). The single cells were measured by a four-probe method using Ag wires as the leads. The measurements were taken using H$_2$ with 3 vol% H$_2$O as fuel and ambient air as oxidant. The cell temperature was first increased to 900 °C and held for two hours to complete the reduction of the anode, and then decreased to 850 °C, 800 °C, and 750 °C for subsequent cell performance testing. Following this procedure, the fuel was switched to propane with 3 vol% H$_2$O and the cell performance was examined in the temperature range of 750—850 °C. The stability testing of the fuel cell under propane fuel (C$_3$H$_8$ with 3 vol% H$_2$O) was performed in two stages: i) an initial 20 h test under the open circuit mode at 800 °C, and ii) continued testing for 60 h under a constant current mode with a 0.4 A cm^{-2} current applied at 850 °C.

3. Results and discussion

3.1. Structure of PSCFN

Fig. 1 shows that the as-synthesized PSCFN has a cubic perovskite (Pm-3m) structure without impurities. The citrate combustion method is more appropriate to synthesize compounds containing several kinds of elements, because the citrate acid acts as a chelator which binds together all the metal ions. After exposure to reducing conditions (H$_2$, 900 °C) the perovskite peaks were altered and additional peaks appeared in the XRD spectra. Compared to several similar compounds such as Sr$_3$Fe$_{1.8}$Co$_{0.2}$O$_{7-\delta}$, Sr$_3$Fe$_{2-x}$Co$_x$O$_{7-\delta}$, and (La,Sr)$_3$(Fe,Ni)$_2$O$_{7-\delta}$ [30—32], the reduced PSCFN spectra displayed in Fig. 1 reveals that it may be a Ruddlesden—Popper (RP) phase with general formula of A$_{n+1}$B$_n$O$_{3n+1}$ [33]. RP phase consists of a
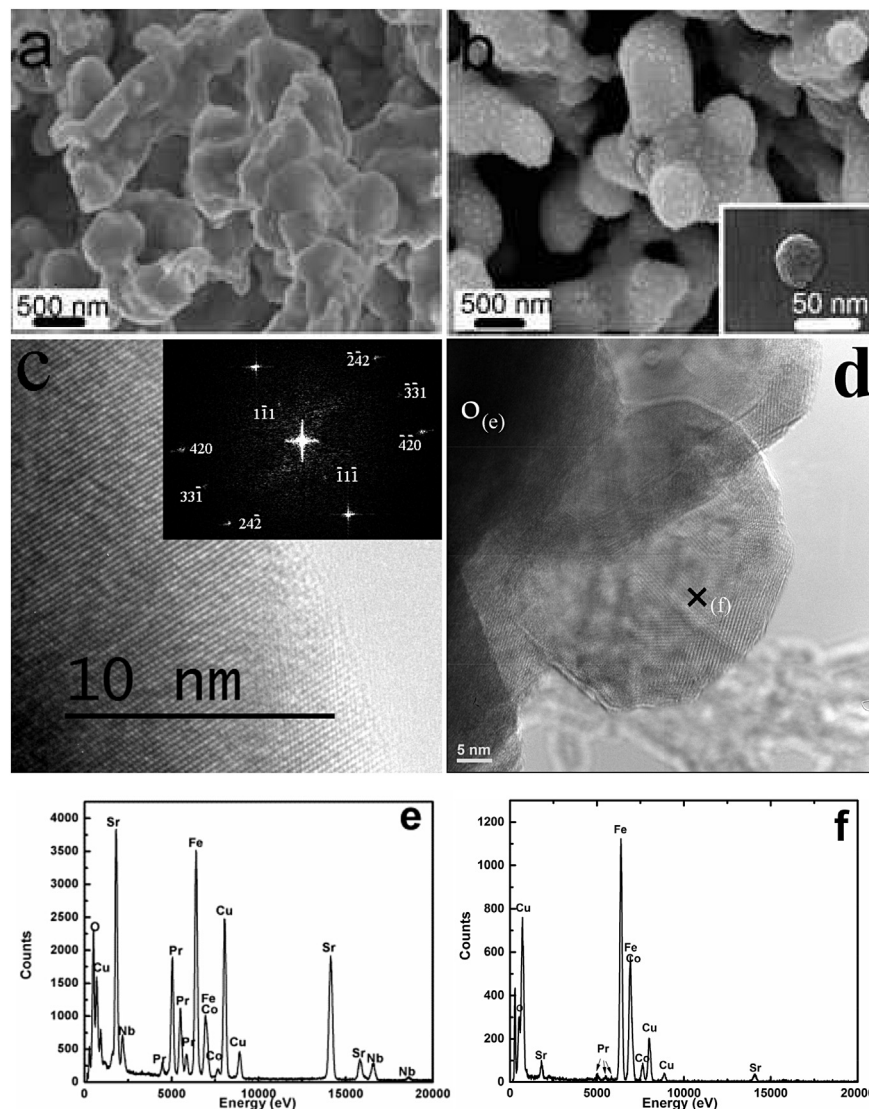

Fig. 2. SEM (a, b) and TEM (c, d) images of PSCFN powders before (a, c) and after (b, d) reduction. EDS of the reduced PSCFN powders on selected area of matrix (e) (marked by O in d) and nanoparticles (f) (marked by × in d).
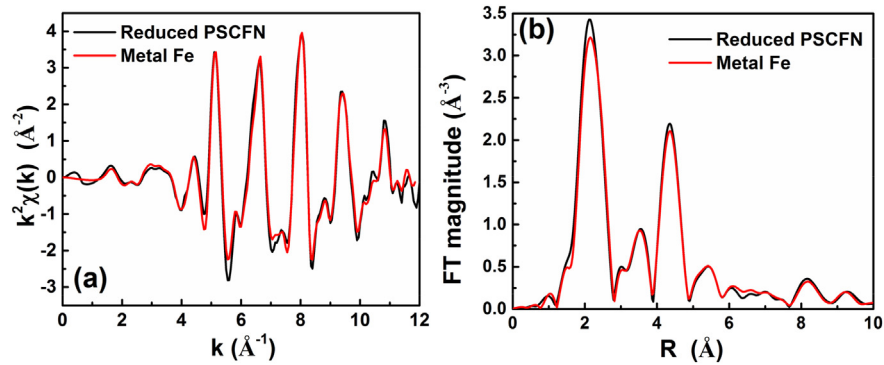
Fig. 3. k^2-weighted EXAFS spectra of Co K-edge in reduced PSCFN and Fe K-edge in metal Fe. (a) k-space data; (b) Fourier transform magnitude.

number of ABO_3 perovskite layers with $n = 1, 2, 3, \dots \infty$, separated by insulating rock-salt layers AO [33,34]. Usually the RP series with different n have similar X-ray diffraction spectra [35,36]. Consequently, it is difficult to determine the exact number of n. Therefore, further studies were conducted as discussed in the following sections. Comparison of the spectra from Fig. 1 with XRD database, it looks similar to $Sr_2(Co/Nb)O_4$ (PDF# 1-70-3973), with the exception of the two peaks at 39.85° and 44.75° (labeled as * in Fig. 1). According to the XRD database, the peaks around 39.85° and 44.75° correspond to the Co—Fe alloy (PDF# 44-1433), indicating that part of the Co and Fe were reduced into metallic phase in the reducing atmosphere.

Fig. 2a and b displays the SEM images of the PSCFN electrodes before and after the reduction process. As shown in Fig. 2a, the as-synthesized PSCFN electrode was homogeneous with a grain size in the submicron range. After reduction, it was observed that besides the main skeleton which shows similar morphology as the synthesized powders, spherical particles with a diameter of approximately 50 nm were uniformly distributed on the surface of the original framework. It is clear that after reduction, the single phase PSCFN had transformed to a structure containing two different phases, which is consistent with the XRD results.

Fig. 2c and d presents the high-resolution transmission electron microscopy (HRTEM) of the PSCFN powders before and after reduction, respectively. Fig. 2c is the TEM image of the as-synthesized PSCFN powder observed along [$\bar{1}$13] zone axis. The measured d-spacing of the (420) planes is 0.159 nm, consistent with the XRD results that a d-spacing of 0.157 nm was obtained for the (210) peak. After reduction, Fig. 2d reveals two different phases similar to the observation of the SEM results in Fig. 2b. Within a single nanoparticle no grain boundary was observable through different

orientation/ordering in the TEM image, implying that the nanoparticle contains only one substance with different orientation/ordering [37,38].

In order to investigate the composition of the reduced PSCFN, TEM-EDS was used on the selected areas of the matrix and the nanoparticles. In Fig. 2e, for the parent matrix all the five elements of Pr, Sr, Co, Fe, Nb can be detected, while Cu in the spectrum comes from the copper TEM sample holder. Compared with the standard database, the Co peak is very weak, implying a significant decrease in the content of Co from the original PSCFN composition. In Fig. 2f, it is clear that the main elements of the nanoparticles are Co and Fe besides trace amounts of Pr and Sr. Consequently, the nanoparticles formed from the in-situ reduction of PSCFN are compounds composed mainly of cobalt and iron and further studies are needed to investigate their local structure and catalytic effect.

The metal Co is a hcp (Hexagonal Close Packed) structure which is distinct from the metallic Fe which possesses a bcc (Body-Centered Cubic) structure. Fig. 3 displays the EXAFS (extended X-ray absorption fine structure) spectra (k^2-weighted) (a) and the corresponding Fourier transforms (b) for the reduced PSCFN. Analysis of the Co-edge demonstrates that the reduced PSCFN shows the same structural characteristics as those of the metallic Fe, indicating that the local environment of Co in the reduced PSCFN is similar to that of the metallic Fe, which is a bcc structure. It appears that all of the Co originally in the perovskite PSCFN was reduced to a metal; this result is consistent with the EDX analysis of the very low Co signal in the parent matrix after reduction. The bimetallic alloy therefore has the bcc structure of Fe, and Co partially replaces Fe atoms in the lattice.

Fig. 4 displays the Fourier transformed EXAFS spectrum of the reduced PSCFN at the Fe k edge shown together with metallic Fe
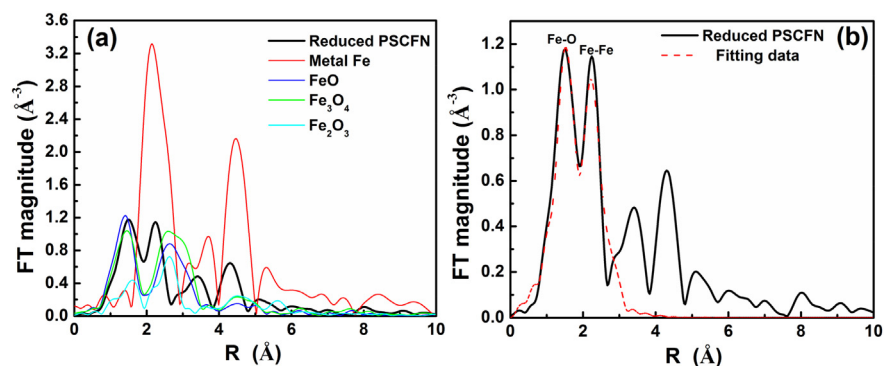

Fig. 4. Fourier transform magnitudes of the EXAFS data (a) Fe K-edge in reduced PSCFN, metal Fe, FeO, Fe_3O_4, and Fe_2O_3; (b) Fe K-edge in reduced PSCFN and best fit for the Fe—Fe (fitting range 1—2.663 Å).
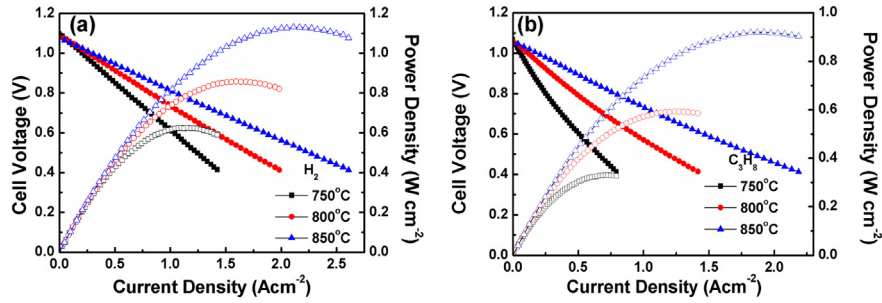
Fig. 5. Single cells composed of PSCFN//LSGM//BCFN with H_2 (a) or C_3H_8 (b) (both with 3 vol% H_2O) as fuel tested at 750, 800, and 850 °C.

and iron oxides (FeO, Fe_2O_3, Fe_3O_4). The spectrum of reduced PSCFN showed two major contributions, one located around 1.5 Å and the second located around 2.3 Å. The peak at 1.5 Å corresponds to the oxygen coordination around iron, which can be observed in the three iron oxides. The second principal peak around 2.3 Å corresponds to the Fe–Fe contribution which displays the same features in reduced PSCFN as that in metallic Fe [39]. This indicates that the Fe in the reduced PSCFN is a mixture of metallic Fe and Fe in other oxidation states. In order to investigate how much Fe was reduced from the perovskite PSCFN, the Fe–Fe signal at 2.3 Å in R space was fitted using IFEFFIT software package [40]. The Fe in the alloy is metallic in nature and is found to possess the bcc structure, with 8 first nearest neighbors and 6 second nearest neighbors. In order to estimate the amount of the reduced states, the volume fraction of Fe^{0+} after reduction was assumed to be x, the coordination number (CN) of the first nearest neighbors was 8*x and the CN of the second nearest neighbors was 6*x. The result of the fitting shows that x is 0.213 ± 0.023, corresponding to approximately 20% of the Fe as metal in the reduced PSCFN. Since all the Co in the PSCFN was reduced to a metallic state, and the original stoichiometric ratio of PSCFN is $PSCo_{0.2}Fe_{0.7}N$, and the ratio of Co:Fe in the alloy would be 0.2/(0.7 × 20%) = 59/41, indicating that Co content in the alloy is approximately 60%. The phase diagram of the Fe–Co binary system with 60% Co indicates that an α phase with a bcc structure is thermodynamically stable below 920 °C, which is consistent with the observation in our experiment [41].

Both SEM and TEM results indicate that PSCFN after reduction contains two different structures. EDS analysis showed that the nanoparticles consist of cobalt and iron. XRD spectra indicate that the reduced PSCFN is a Ruddlesden–Popper phase combined with Co–Fe alloy phase. XAFS results have demonstrated that the Co–Fe alloy is bcc structure with Co:Fe ratio of 59:41 and all the Co was reduced into the metallic phase. Therefore, the remaining parent

fraction is $(Pr_{0.4}Sr_{0.6})_3(Fe_{0.85}Nb_{0.15})_2O_{7+\delta}$ of the RP phase and the nanoparticles are bimetallic alloy of $Co_{0.59}Fe_{0.41}$.

An important implication of this material behavior under reducing conditions expected in the SOFC anodes is that the bimetallic alloys can be produced in-situ under the fuel cell operating conditions leading to a homogenous distribution of catalytic sites. Compared with a mechanical mixture of powders from the electrode fabrication process [42,43], or an infiltration method after the formation the electrode framework [44,45], in-situ synthesis of metal alloy catalytic sites in our work are easier to achieve and provides a unique opportunity for obtaining a uniform distribution of the catalyst phase.

The search for new mixed-conductor oxides with enhanced structural stability than the perovskite phases has led to the exploration of the mixed-conductor properties of the Ruddlesden-Popper series having the general formula of $A_{n+1}B_nO_{3n+1}$. The crystal structure of these materials consists of n perovskite layers of ABO_3 alternated with AO rock-salt layers [30,31]. It has been shown that reduction of PSCFN leads to the formation of a novel dual phase anode material consisting of a parent oxide with a Ruddlesden–Popper structure and a bimetallic Co–Fe alloy. The SOFC cell performance and catalytic activity of this composite material system will be explored in the following section.

3.2. Cell performance

Fig. 5a) displays the single fuel cell performance with H_2 (3 vol% H_2O) supplied to the anode and ambient air supplied to the cathode in the temperature range of 750 °C to 850 °C. The open circuit voltage (OCV) was 1.1 V while the maximum cell power density reached 0.62, 0.86, and 1.13 W cm^{-2} at 750, 800, and 850 °C, respectively. After switching the fuel from H_2 to C_3H_8 (3 vol% H_2O), the OCV dropped slightly while the maximum cell power density could reach 0.33, 0.59, and 0.92 W cm^{-2} at 750, 800, and 850 °C, respectively. This cell performance is comparable to the Ni modified anode using direct propane as a fuel [12,46–48]. As described above, the current anode materials consists of two phases, a layered $(Pr_{0.4}Sr_{0.6})_3(Fe_{0.85}Nb_{0.15})_2O_{7+\delta}$ and a Co–Fe bimetallic alloy. In many previous reports, materials with Ruddlesden–Popper phases such as $Sr_3Fe_2O_{6+\delta}$ usually have high conductivity with p type charge carriers and the electronic transport properties are attributed to the presence of electron holes localized on the iron sites [49]. The oxide component of the anode material in this study, the
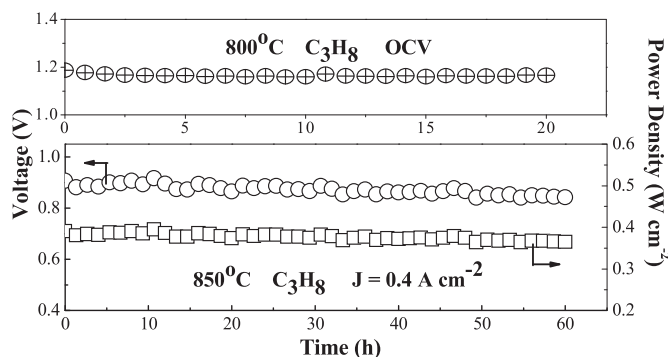

Fig. 6. Stability test using C_3H_8 as fuel with first 20 h in OCV mode and 60 h with 0.4 A cm^{-2} current applied.

Table 1
Chemical products with their mass-to-charge ratio.

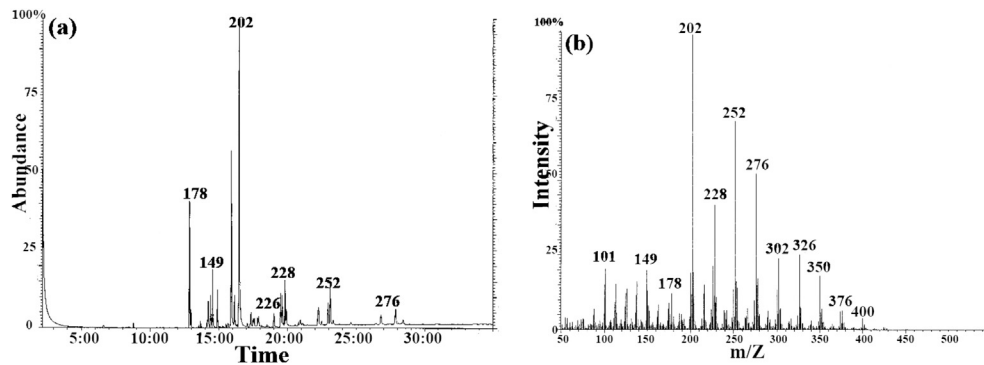| m/z	178	202	228	252	276	149
Chemicals	Anthracene	Pyrene and fluoranthene	Chrysene	Benzo	Dibenzo chrysene	Plastic bag

Fig. 7. Gas chromatography–mass spectrometry (GC–MS) testing of the chemicals. Different peaks with time (a) and different mass-to-charge ratio (b).

$(Pr_{0.4}Sr_{0.6})_3(Fe_{0.85}Nb_{0.15})_2O_{7+\delta}$ has a high conductivity which is appropriate for the electrode [50]. The Co–Fe bimetallic alloy is metal with high electronic conductivity and usually has an excellent catalytic performance, especially in the Fischer–Tropsch synthesis [23,24,50]. The combination of the high conductive oxide matrix and the excellent catalytic activity of the Co–Fe metallic phase has led to high cell power output with both hydrogen and propane fuels.

The durability testing of the cell was conducted with 20 h in the OCV mode at 800 °C and 60 h with 0.4 A cm^{-2} current applied at 850 °C. The cell performance was stable during the 80 h testing as shown in Fig. 6, suggesting that the composite anode can direct oxidize propane without coking compared with the conventional anode material such as Ni–YSZ which degrades quickly in hydrocarbons fuels [13,51]. Meanwhile the long term stability confirms that the RP phase is stable at reducing conditions at the cell operating temperature.

3.3. Analysis of the chemical products

During the 80 h durability test using propane as fuel, thick and viscous yellowish liquid was collected in the exhaust stream of the fuel cell. After characterization using gas chromatography–mass spectrometry, macromolecular compounds containing a benzene ring were detected. These compounds with different mass-to-charge ratio (m/z) are listed in Table 1. Fig. 7a displays the GC–MS spectra of different peaks with time which correspond to compounds with different mass-to-charge ratio weight (Fig. 7b). The polycyclic aromatic hydrocarbons (PAHs) found in the liquid state at the conclusion of cell testing were the products of the
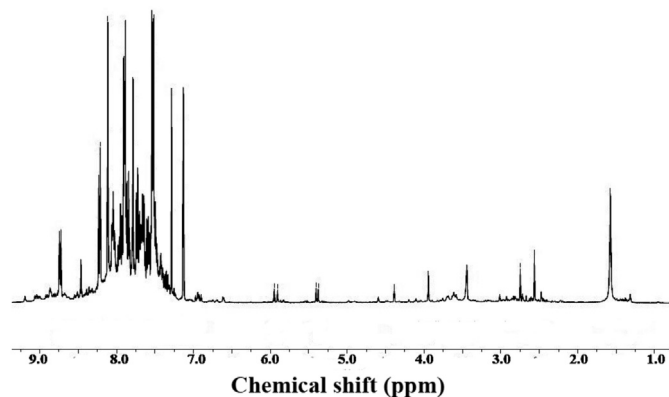
propane-fueled SOFCs using the composite anode with the Co–Fe bimetallic catalyst.

Fig. 8 shows ^{1}H NMR spectrum of the by-product of the direct propane fueled SOFCs. The ^{1}H NMR reveals the structure of a molecule by the chemical shift (δ), which provides information of the chemical environment of the protons. The signature resonances of the protons in benzene is located at $\delta = 7.27$ ppm [52], while the protons in PAHs usually have a characteristic δ in the range of 6.3–8.5 ppm. In Fig. 8 the peaks around 7.2–8.3 ppm indicate most of the protons are on the benzene ring of PAHs. Since these peaks are complex, including several sets of compounds and their isomers with protons in different environment, the by-product must be a mixture of several kinds of PAHs. These results confirm the results of the GC–MS tests.

Evidence of PAH compounds were also confirmed in the infrared spectrum, as shown in Fig. 9. The absorption peak around 3100–3000 cm^{-1} and 910–670 cm^{-1} corresponds to the stretching vibration of the ν_{C-H} and bending vibration of the δ_{C-H} of the C–H on the benzene ring. The peaks around 1600 cm^{-1} and 1500 cm^{-1} are the stretching vibrations of the $\nu_{C=C}$ benzene skeleton [53]. Similar to the NMR results, the main peak shows an overlap with many small peaks, indicating this must be a complex mixture of compounds containing several kinds of PAHs.

The collection of GC–MS, NMR and IR data shows that there are PAH chemicals in the products of direct propane fueled SOFCs using a novel dual phase anode material formed by reduction of a PSCFN material. In this electrochemical reaction occurring in the presence
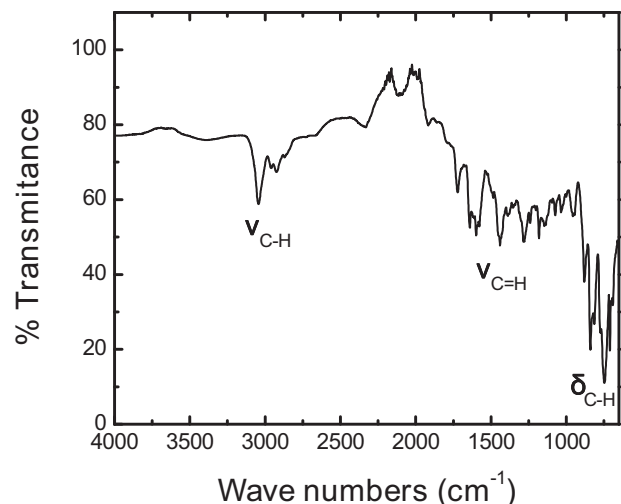

Fig. 8. ^{1}H nuclear magnetic resonance (NMR) spectrum of the chemicals produced in the SOFC exhaust stream.

Fig. 9. Infrared (IR) spectroscopy of the chemical products.

of the Co–Fe catalyst operating at 850 °C, macromolecular compounds were found as liquid products, which were different from the traditional Fischer–Tropsch synthesis occurring at lower temperature in the 150–350 °C range producing small molecule product such as alkenes or alcohols. The operating temperature of the SOFCs is in the range of 750–850 °C, which is much higher than the typical temperature of FT synthesis. On one hand, the high operating temperature offers energy for dehydrogenating of hydrocarbon, especially the energy for breaking the C–H bond. On the other hand, the applied current (0.4 A cm^{-2} in this study) accelerates the electronic transport in the electrode which may benefit the formation of a benzene ring. The metal alloy in the anode is cobalt and iron, which are the two most common catalysts for the FT synthesis. Cobalt is the preferred catalyst in the FT synthesis of higher hydrocarbons due to its high activity and selectivity, low water-gas shift activity, and resistance towards deactivation [54]. Usually cobalt catalysts produce high yields of long-chain alkenes in the FT synthesis [55]. Iron catalyst development has focused on improving the catalytic activity in the lower temperature regime where most of the hydrocarbon product is in the liquid phase under reaction conditions [23]. In many previous reports, Fe–Co alloys were used as catalyst for dehydrogenation in the Fischer–Tropsch synthesis. Qiu and co-workers found that in the dehydrogenation of ammonia borane at room temperature, the in situ synthesized $Fe_{0.3}Co_{0.7}$ alloys exhibit excellent catalytic properties [56]. Wang et al. have predicted the formation of the aromatic products from C_2H_4, C_4H_6, and C_4H_6 through modeling of the steam cracking of F–T naphtha [57]. The incorporation of cobalt and iron phases results in substantial changes in both activity and product distribution. When used together, they do not simply give the additive properties (activity, selectivity) expected from knowledge of the properties of the individual metals [55]. These bimetallic Co–Fe catalysts have been shown to be much more attractive in terms of alcohol formation and give rise to the production of ethanol and propanol, depending on the iron content [58]. The possible interaction of cobalt and iron in the alloys when used as anode catalyst in SOFCs at high operating temperatures in the present case and the applied current during the SOFC operation may accelerate the catalytic processes that yield the formation of PAHs.

For these PAHs, they can be valuable in many industrial applications. Anthracene is an organic semiconductor used as a scintillator for detectors of high energy photons, electrons and alpha particles [59,60]. It is also used in wood preservatives, insecticides, and coating materials. Chrysene and pyrene are used commercially to make dyes and dye precursors. The significance of this study has been the demonstration of the formation of the PAHs from the small molecular hydrocarbons through electrochemical reaction in the SOFC system. The PAHs are liquid at ambient temperature and pressure, making it convenient for transport and storage.

4. Conclusions

PSCFN starting materials used as SOFC anodes changed to a dual phase system consisting of $(Pr_{0.4}Sr_{0.6})_3(Fe_{0.84}Nb_{0.15})_2O_{7+\delta}$ covered with Co–Fe nanoparticles after reduction in H_2 at elevated temperatures. XAFS results indicated that the Co–Fe bimetallic alloy was composed of 59:41 mol% of Co and Fe, and the alloy possessed the same bcc structure as that of the metallic Fe. SOFCs employing this novel anode material demonstrated high cell power output with either H_2 or C_3H_8 as fuel. Durability testing indicated that the stability with propane at 850 °C was excellent with no evidence of coking induced cell degradation. GC–MS, NMR and IR data showed the existence of PAHs in the product of direct propane SOFCs with $(Pr_{0.4}Sr_{0.6})_3(Fe_{0.85}Nb_{0.15})_2O_{7+\delta}$ anode containing Co–Fe alloy. These macromolecular compounds are produced as by-products during operation of SOFCs for power generation. This novel material system successfully demonstrated co-generation of electricity and high value end use chemicals (PAHs) from direct hydrocarbon fueled SOFC systems.

References

[1] S.C. Singhal, Solid State Ionics 135 (2000) 305–313.
[2] A.B. Stambouli, E. Traversa, Renew. Sustain. Energy Rev. 6 (2002) 433–455.
[3] W. Wiyaratn, Eng. J. 14 (2010) 1–14.
[4] F. Alcaide, P. Cabot, E. Brillas, J. Power Sources 153 (2006) 47–60.
[5] R.D. Farr, C.G. Vayenas, J. Electrochem. Soc. 127 (1980) 1478–1483.
[6] I.V. Yentekakis, C.G. Vayenas, J. Electrochem. Soc. 136 (1989) 996–1002.
[7] S. Neophytides, C.G. Vayenas, J. Electrochem. Soc. 137 (1990) 839–845.
[8] D.J. Moon, J.M. Park, J.S. Kang, K.S. Yoo, S.I. Hong, J. Ind. Eng. Chem. 12 (2006) 149–155.
[9] W. Wiyaratn, W. Appamana, S. Charojrochkul, S. Kaewkuekool, S. Assabumrungrat, J. Ind. Eng. Chem. 18 (2012) 1819–1823.
[10] S. Moret, L.S. Conte, J. Chromatogr. A 882 (2000) 245–253.
[11] H. Hampikyan, H. Colak, Asian J. Chem. 22 (2010) 5797–5807.
[12] S.P. Jiang, S.H. Chan, J. Mater. Sci. 39 (2004) 4405–4439.
[13] S. McIntosh, R.J. Gorte, Chem. Rev. 104 (2004) 4845–4865.
[14] W. Wang, S.P. Jiang, A.I.Y. Tok, L.H. Luo, J. Power Sources 159 (2006) 68–72.
[15] D. Ding, Z.B. Liu, L. Li, C.R. Xia, Electrochem. Commun. 10 (2008) 1295–1298.
[16] L. Yang, Y.M. Choi, W.T. Qin, H.Y. Chen, K. Blinn, M.F. Liu, P. Liu, J.M. Bai, T.A. Tyson, M.L. Liu, Nat. Commun. 2 (2011) 357.
[17] S.D. Park, J.M. Vohs, R.J. Gorte, Nature 404 (2000) 265–267.
[18] Z.L. Zhan, S.A. Barnett, Science 308 (2005) 844–847.
[19] S.W. Tao, J.T.S. Irvine, Nat. Mater. 2 (2003) 320–323.
[20] Q. Liu, X.H. Dong, G.L. Xiao, F. Zhao, F.L. Chen, Adv. Mater. 22 (2010) 5478–5482.
[21] Y.H. Huang, G. Liang, M. Croft, M. Lehtimäki, M. Karppinen, J.B. Goodenough, Chem. Mater. 21 (2009) 2319–2326.
[22] C.H. Yang, Z.B. Yang, C. Jin, G.L. Xiao, F.L. Chen, M.F. Han, Adv. Mater. 24 (2012) 1439–1443.
[23] H. Schulz, Appl. Catal. A: Gen. 186 (1999) 3–12.
[24] G.P. Van Der Laan, A.A.C.M. Beenackers, Catal. Rev. Sci. Eng. 41 (1999) 255–318.
[25] V.A. de la Pena O'Shea, M.C. Álvarez-Galván, J.M. Campos-Martín, J.L.G. Fierro, Appl. Catal. A: Gen. 326 (2007) 65–73.
[26] C. Knottenbelt, Catal. Today 71 (2002) 437–445.
[27] T. Kaneko, F. Derbyshire, E. Makino, D. Gray, M. Tamura, Coal Liquefaction in Ullmann's Encyclopedia of Industrial Chemistry, Wiley-VCH, Weinheim, 2001, http://dx.doi.org/10.1002/14356007.a07_197.
[28] K.Q. Huang, R.S. Tichy, J.B. Goodenough, J. Am. Ceram. Soc. 81 (1998) 2565–2575.
[29] Z.B. Yang, C.H. Yang, C. Jin, M.F. Han, F.L. Chen, Electrochem. Commun. 13 (2011) 882–885.
[30] S.G.P. Adler, Solid State Commun. 116 (2000) 585–589.
[31] F. Prado, A. Manthiram, J. Solid State Chem. 158 (2001) 307–314.
[32] L. Mogni, F. Prado, A. Caneiro, A. Manthiram, Solid State Ionics 177 (2006) 1807–1810.
[33] S.N. Ruddlesden, P. Popper, Acta Cryst. 1 (1958) 54–55.
[34] S.N. Ruddlesden, P. Popper, Acta Cryst. 10 (1957) 538–539.
[35] F. Sher, A.J. Williams, A. Venimadhev, M.G. Blamire, J.P. Attfield, Chem. Mater. 17 (2005) 1792–1796.
[36] J.H. Haeni, C.D. Theis, D.G. Schlom, W. Tian, X.Q. Pan, H. Chang, I. Takeuchi, X.D. Xiang, Appl. Phys. Lett. 78 (2001) 3292–3294.
[37] S.G. Martín, D.P. Fagg, J.T.S. Irvine, Chem. Mater. 20 (2008) 5933–5938.
[38] Z.P. Li, T. Mori, F. Ye, D.R. Ou, G.J. Auchterlonie, J. Zhou, J. Drennan, J. Phys. Chem. C 116 (2012) 5435–5443.
[39] A.A. Battiston, J.H. Bitter, D.C. Koningsberger, Catal. Lett. 66 (2000) 75–79.
[40] M. Newville, J. Synchrotron Rad. 8 (2001) 322–324.

[41] I. Ohnuma, H. Enokia, O. Ikeda, R. Kainuma, H. Ohtani, B. Sundman, K. Ishida, Acta Mater. 50 (2002) 379–393.
[42] C.R. Xia, Y.L. Zhang, M.L. Liu, Appl. Phys. Lett. 82 (2003) 901–903.
[43] K. Eguchi, J. Alloys Compd. 250 (1997) 486–491.
[44] H. Kim, C. Lu, W.L. Worrell, J.M. Vohs, R.J. Gorte, J. Electrochem. Soc. 149 (2002) A247–A250.
[45] H. Uchida, H. Suzuki, M. Watanabe, J. Electrochem. Soc. 145 (1998) 615–620.
[46] Z.L. Zhan, J. Liu, S.A. Barnett, Appl. Catal. A: Gen. 262 (2004) 255–259.
[47] Z.P. Shao, S.M. Haile, J. Ahn, P.D. Ronney, Z. Zhan, S.A. Barnett, Nature 435 (2005) 795–798.
[48] M.L. Faro, D.L. Rosa, I. Nicotera, V. Antonucci, A.S. Arico, Appl. Catal. B: Environ. 89 (2009) 49–57.
[49] L. Mogni, N. Grunbaum, F. Prado, A. Caneiro, J. Electrochem. Soc. 158 (2011) B202–B207.
[50] D. Leckel, Energy Fuel 23 (2009) 2342–2358.
[51] M. Mogensen, K. Kammer, Ann. Rev. Mater. Res. 33 (2003) 321–331.
[52] J. Clayden, N. Greeves, S. Warren, Organic Chemistry, University Press, Oxford, ISBN: 978-0199270293.
[53] B. Stuart, Infrared Spectroscopy Fundamentals and Applications, Wiley.
[54] C. Aaseruda, A.M. Hilmen, E. Bergene, S. Eric, D. Schanke, A. Holmen, Catal. Lett. 94 (2004) 171–176.
[55] V.A. de la Peña O'Shea, M.C. Álvarez-Galván, J.M. Campos-Martin, N.N. Menéndez, J.D. Tornero, J.L.G. Fierro, Eur. J. Inorg. Chem. (2006) 5057–5068.
[56] F.Y. Qiu, Y.J. Wang, Y.P. Wang, L. Li, G. Liu, C. Yan, L.F. Jiao, H.T. Yuan, Catal. Today 170 (2011) 64–68.
[57] F. Wang, Y. Xu, J. Ren, Y. Li, Chem. Eng. Process 49 (2010) 51–58.
[58] V.A. de la Peña O'Shea, N.N. Menéndez, J.D. Tornero, J.L.G. Fierro, Catal. Lett. 88 (2003) 123–128.
[59] N. Balamurugan, A. Arulchakkaravarthi, P. Ramasamy, Nucl. Instrum. Meth. Phys. Res. A 568 (2006) 767–771.
[60] N. Balamurugan, A. Arulchakkaravarthi, P. Ramasamy, Phys. Stat. Sol. A 204 (2007) 3502–3508.